

Supporting Information

Transient and dry recycling of battery materials with negligible carbon footprint and roll-to-roll scalability

Hao Zhang^{1,#}, Yongsheng Ji^{1,#}, Yonggang Yao^{1,*}, Long Qie^{1,*}, Zhiheng Cheng¹, Zhihao Ma², Xin Qian², Ronggui Yang², Chenghang Li³, Yaqing Guo^{1,3}, Yifei Yuan³, Haoyu Xiao², Haiping Yang², Jing Ma¹, Jun Lu^{4,*}, Yunhui Huang^{1,*}

¹State Key Laboratory of Materials Processing and Die & Mould Technology, School of Materials Science and Engineering, Huazhong University of Science and Technology, Wuhan, 430074 China

²State Key Laboratory of Coal Combustion, School of Energy and Power Engineering, Huazhong University of Science and Technology, Wuhan, 430074, China

³College of Chemistry and Materials Engineering, Wenzhou University, Wenzhou, 325035 China

⁴College of Chemical and Biological Engineering, Zhejiang University, Hangzhou, 310027, China

This supporting information contains:

- Experimental methods
- Figures S1-S24
- Tables S1-S6
- Supplementary Movie S1

Experimental methods

Recycling process

Spent batteries are discharged to less than 1 V for safety concerns. Anode electrodes were then manually split out from the discharged batteries in the argon-filled glovebox. The exhausted anodes were cut into pieces before shock-type heating. The anode pieces were heated with various kinds of parameters settings for different temperatures and duration time, the HT graphite could be obtained. For regeneration, HT graphite was first purified with 2M H₂SO₄ for 1h and then washed three times with super-pure water before drying in the oven at 80 °C for 12h. To repair the surface structure, the graphite was further coated with amorphous carbon through carbonization of PAN coating at 1100 °C with argon gas protection for 2h, then regenerated graphite was acquired. Spent graphite powder was just scraped from the exhausted anode. Graphite was stripped down from anode scrap through shock-type and rolled-over heating treatment so that scrap graphite was obtained. Similarly, all spent cathode powders are scraped from spent electrodes carefully in a manual way. All recycled cathode materials were obtained through our shock-type heating method. Additionally, the recycled LCO powders were further regenerated through a combination method of hydrothermal treatment and short-time annealing.

Material characterizations.

SEM (SEM, Zeiss Sigma 300) was employed to obtain information on particle morphology. The phase structures were identified by XRD-7000 X-ray diffractometer (Shimadzu, Japan) with a scanning speed of 10°/min (Cu K α radiation, $\lambda = 1.5406 \text{ \AA}$). The HRTEM observation was performed at a Field Emission Transmission Electron Microscope (Talos F200X). Raman spectra were obtained using a LabRAM HR800. The elemental composition of graphite was evaluated by inductively coupled plasma–optical emission spectrometry (ICP–OES, Agilent ICPMS 7700). The

particle size distribution was measured by a particle size analyzer (Mastersizer 3000). Thermogravimetric analysis (TGA, STA449F3) was performed from 35 to 950 °C (heating rate of 10 °C min⁻¹) in an argon atmosphere. FTIR spectra were collected by a Nicolet iS50R from 400 to 4000 cm⁻¹.

Recovery efficiency calculation.

The recovery efficiencies of recycled materials (anode and cathode) are calculated according to the equation bellowing by sample mass.

$$\sigma_c = (M_0 - m_{Al}) / (M_0 - M_{Al})$$

where σ_c is the recycling efficiency of cathode materials, M_0 is the mass of the electrode piece, m_{Al} is the mass of the separated aluminum foil piece through the shock-type heating, M_{Al} is the mass of the pure aluminum foil.

$$\sigma_G = (M_0 - m_{Cu}) / (M_0 - M_{Cu})$$

$$\sigma_{Cu} = m_{1,Cu} / M_{Cu}$$

where σ_G is the recycling efficiency of graphite, M_0 is the mass of the electrode piece, m_{Cu} is the mass of the separated copper foil piece through the shock-type heating, M_{Cu} is the mass of the pure copper foil, σ_{Cu} is the recycling efficiency of copper foil, $m_{1,Cu}$ is the mass of the separated copper foil after cleaning thoroughly.

Heat transfer analysis

The heat transfer analysis is performed using a one-dimensional approximation since the electrode lengths (~1 cm) are much larger than the thickness (~0.1 mm). The heat transfer model contains several sections, including the airgap, and the electrode with a sandwich structure containing graphite and copper current collectors.

The heat flux injected into the electrode is a coupled radiation, conduction, and natural convection process. First, radiation heat transfer across the air gap can be calculated as:

$$q_{rad} = \frac{\sigma(T_1^4 - T_2^4)}{\frac{1 - \epsilon_1}{\epsilon_1} + \frac{1}{F_{1,2}} + \frac{1 - \epsilon_2}{\epsilon_2}} \quad (1)$$

where σ is the Stefan-Boltzmann constant; T_1 is the time-dependent temperature of the heater; T_2 is the temperature of the graphite surface 2; $\epsilon_{1/2}$ is the emissivity of the heater/graphite; $F_{1,2}$ is the view factor between the heater and the graphite, which can be found in the table of view factor for radiation between parallel rectangles. In the air gap, the conductive and convective heat transfer could be presented by the effective thermal conductivity k_e :

$$\frac{k_e}{k} = C(Gr_\delta Pr)^n \left(\frac{L}{\delta}\right)^m \quad (2)$$

where k is the thermal conductivity of the air; L is the length of the airgap; δ is the thickness of the air gap; C , n , and m are constants; $Gr_\delta = \frac{g\beta(T_1 - T_2)\delta^3}{\nu^2}$ is the Grashof number, in which g is the gravitational acceleration, β is the thermal expansion coefficient, and ν is the kinematic viscosity;

$Pr = \frac{\rho c_p \nu}{k}$ is the Prandtl number, in which ρ is the density, c_p is the specific thermal capacity. Due

to the small gap size, the natural convection is negligible, resulting in $\frac{k_e}{k} \approx 1$. Next, the conductive heat transfer both inside the airgap and the electrode can be calculated by solving the heat equation:

$$\rho c_p \frac{\partial T}{\partial t} - k \frac{\partial^2 T}{\partial x^2} = 0 \quad (3)$$

We also consider the interface conductance between the graphite layers and the copper current collector by:

$$T'(t) - T''(t) = \frac{Q(t)}{G} \quad (4)$$

where $T'(t)$ and $T''(t)$ are temperatures of the two sides of the interface; $Q(t)$ is the local heat flux; G is the interface thermal conductance.

To solve the above equations, the boundary condition at position 1 is

$$T_1(t) = T_{heater}(t) \quad (5)$$

At position 5:

$$-k \frac{\partial T}{\partial x} = h(T_5 - T_a) + \frac{\sigma(T_5^4 - T_a^4)}{\frac{1 - \epsilon_5}{\epsilon_5} + \frac{1}{F_{5,a}} + \frac{1 - \epsilon_a}{\epsilon_a}} \quad (6)$$

where h is the convective heat transfer coefficient, and subscript a means the ambient environment.

The detailed parameters we used in the simulation are listed as follows:

Parameters in the COMSOL model	
Parameters	Value
Emissivity of heater ϵ_1	0.8
Emissivity of graphite ϵ_2, ϵ_5	0.76
Emissivity of the ambient ϵ_a	1
View factor $F_{1,2}$	0.2
View factor $F_{5,a}$	1
Length of sample L	0.01 m
Air gap thickness δ	0.01 m
Density of air ρ_a	1 kg/m ³
Specific heat capacitance of air c_{pa}	1200 J/(kg·K)
Thermal conductivity of air k_a	0.08 W/(m ² ·K)
Density of graphite ρ_g	1600 kg/m ³
Specific heat capacitance of graphite c_{pg}	710 J/(kg·K)
Thermal conductivity of graphite k_g	10 W/(m ² ·K)
Density of copper ρ_{co}	8960 kg/m ³
Specific heat capacitance of copper c_{pco}	385 J/(kg·K)
Thermal conductivity of copper k_{co}	400 W/(m ² ·K)
Thermal conductivity of interfaces G	10 ⁶ W/(m ² ·K)

In addition, the time-dependent solver PARDISO (Parallel Direct Solver) was used for solving coupled equations 1-6. A uniform 1D mesh with an element size of 10^{-6} m was built for numerical calculation, and the number of elements is 10132. Results of the temperature distribution along the thickness direction of the electrode are shown in Figure 2f. This uniform temperature distribution can be explained by the Biot number, which reflects the relative magnitudes of surface heat transfer and internal conduction resistances to heat transfer:

$$Bi = \frac{\delta h}{k} \quad (7)$$

where δ is the thickness of the electrode sample, h is the heat transfer coefficient between the sample and the ambient environment, and k is the thermal conductivity of the sample. In this case, we estimated that $Bi \sim 0.001$, such a small Biot number suggests that internal heat conduction dominates over surface heat transfer, and the temperature in the electrode is uniform.

Electrochemical measurements

(a) For anode materials. The anode material was obtained by the homogeneous mixing of active compound (93 wt.%), conductive agent (Super P, 2 wt.%), and binder (PVDF, 5 wt.%) in NMP. Next, the mixture was coated onto a copper foil and dried in a vacuum oven for 12 hours at 80 °C to produce the cathode plate that was cut into round disks (12 mm diameter). The mass loading of active materials was controlled at approximately 2.5 mg/cm². Lithium metal was used as the counter electrode. Porous polypropylene was used as the separator and 1 mol L⁻¹ LiPF₆ (1.0 M) (EC: DEC = 1:1 Vol% with 5% FEC) was used as the electrolyte. Finally, all components were assembled into 2025-type coin cells in an argon-filled glovebox. The just assembled coin cells were held for 12h to ensure a full invasion of electrolytes. Then, the electrochemical performances of active materials were tested using a Neware battery test system. The cycling stability was

studied at a 0.5 C rate ($1\text{ C} = 372\text{ mAh g}^{-1}$) after activating with a 0.1 C rate for three cycles. The cut-off voltages during charging and discharging were set at 1.5 V and 0.01 V (versus Li^+/Li) for all tests.

(b) For cathode materials. To evaluate the electrochemical performance, both R-LCO and S-LCO powders were mixed with PVDF and acetylene black in NMP at a mass ratio of 8:1:1. The resulting slurries were cast on aluminum foils followed by vacuum drying at $90\text{ }^\circ\text{C}$ for 12 h. Circle electrodes were cut and compressed, with a controlled active mass loading of about 3 mg/cm^2 . After 12 h aging of the assembled coin-cells for the full wetting of the electrolyte, the electrochemical tests were performed. Galvanostatic charge–discharge tests were carried out at a current density of 1 C ($1\text{ C} = 150\text{ mA g}^{-1}$) for 100 cycles after three activation cycles at 0.1 C and rate capacity measurement was performed at the current densities of 0.1, 0.2, 0.5, 1, 2, 5, and 10 C in the potential range of 2.8–4.35 V (vs. Li^+/Li) at room temperature.

Environmental and economic analysis

The environmental and economic analyses of the different recycling processes were conducted using an SF-18-022 EverBatt model, developed by the Argonne National Laboratory, USA (www.Anl.Gov/egs/everbatt). The simulation of three methods including pyrometallurgy, hydrometallurgy, and transient recycling is based on the following assumptions. All data relating to energy consumption, waste emission, cost, and revenue were extracted from the “Rec Par.” and “Output” pages. Profit equals revenue minus cost. In detail, energy consumption and cost data are from the “Recycle” and “Recycling cost” tables on the “Output” page, respectively. Waste emission data are from the “Produced materials from recycling” and “Environmental impacts for battery recycling” tables on the “Rec Par.” page. Revenue data are from the “Revenue generated from sales of recycled materials” table on the “Rec Par.” page. For pyrometallurgy and

hydrometallurgy, the environmental and economic data of pyrometallurgical and hydrometallurgical recycling methods can be calculated automatically and extracted directly in the “Pyrometallurgical” and “Hydrometallurgical” parts, respectively. Note that the energy consumption of the smelting process of pyrometallurgy was zero due to the usage of hazardous feed material as fuel. For our transient recycling method, no additional material input (Table S6), and the recovery efficiency are updated according to experimental data, respectively. The electricity consumption was calculated to be 1.06 MJ/kg cell. Then, the data can be calculated through the Everbatt model.

Supporting Figures:

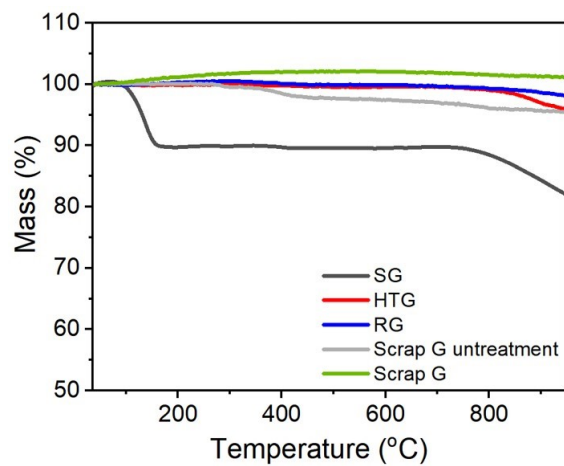


Figure S1. TGA curves for SG and HTG.

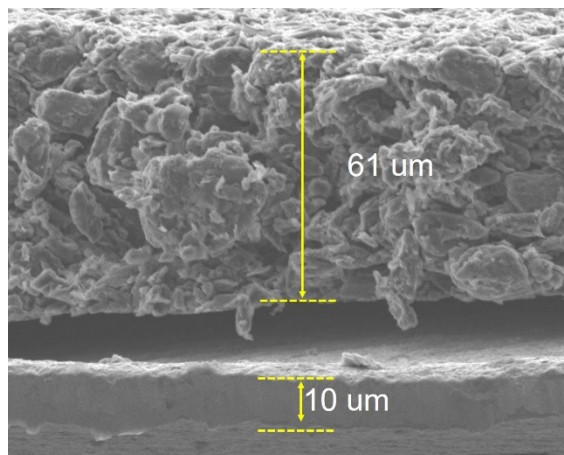


Figure S2. Cross-section SEM image of the undisposed anode electrode.

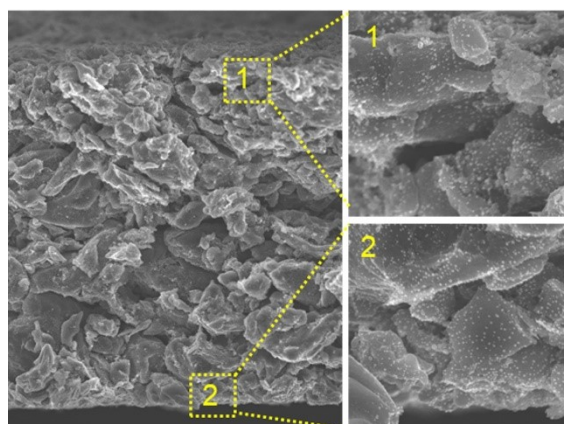


Figure S3. SEM of HTG at the top surface and bottom surface to demonstrate the uniformity.

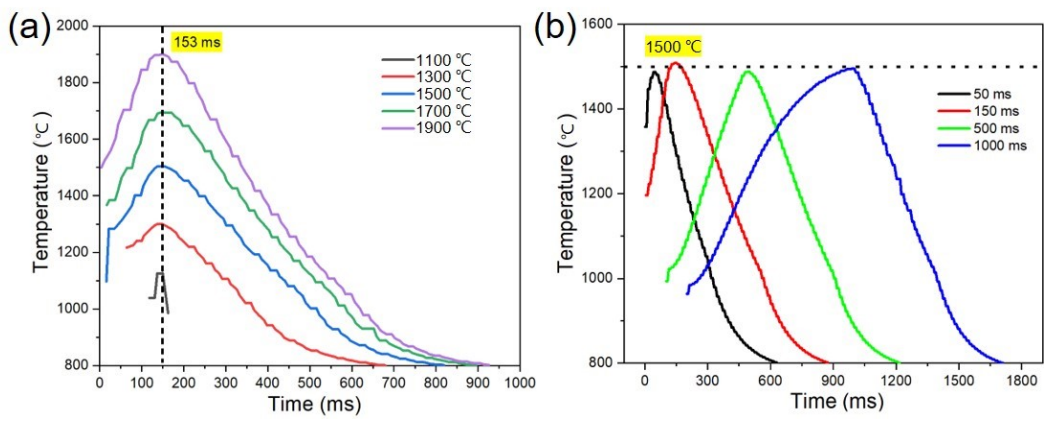


Figure S4. The temperature profile of the heater for (a) different peak temperatures and (b) duration time.

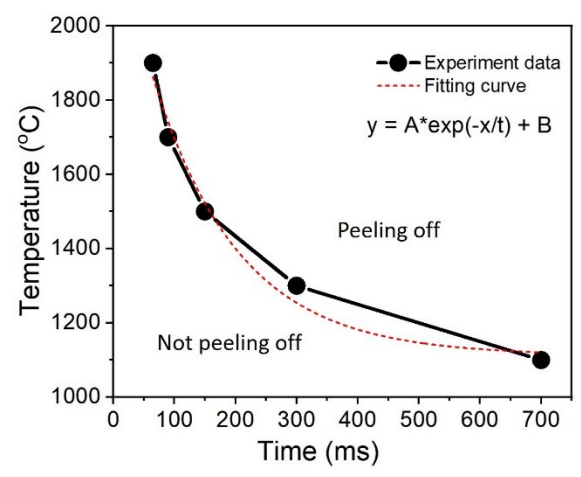


Figure S5. T-t diagram for the graphite recycling from the anode.

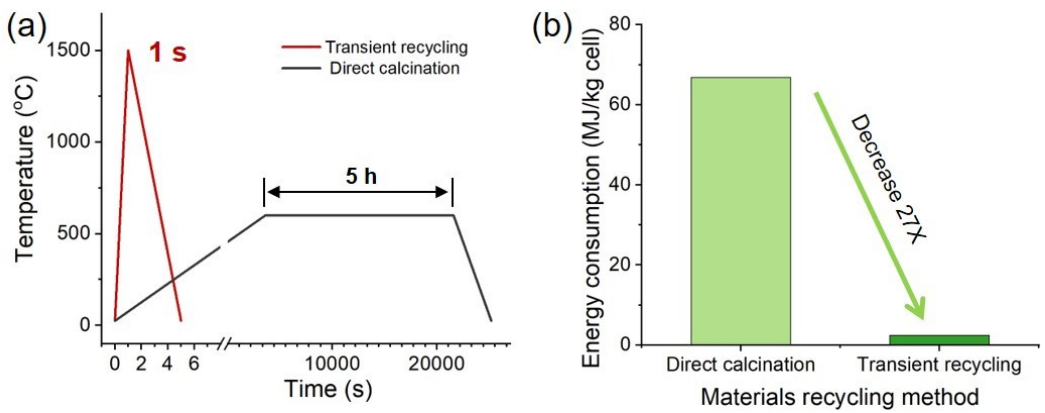


Figure S6. A comparison of the (a) time efficiency and (b) energy consumption of our transient recycling with the direct calcination method.

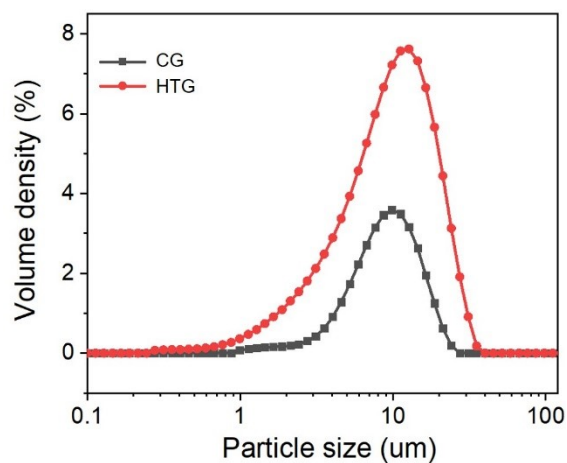


Figure S7. Size distribution of HTG and CG.

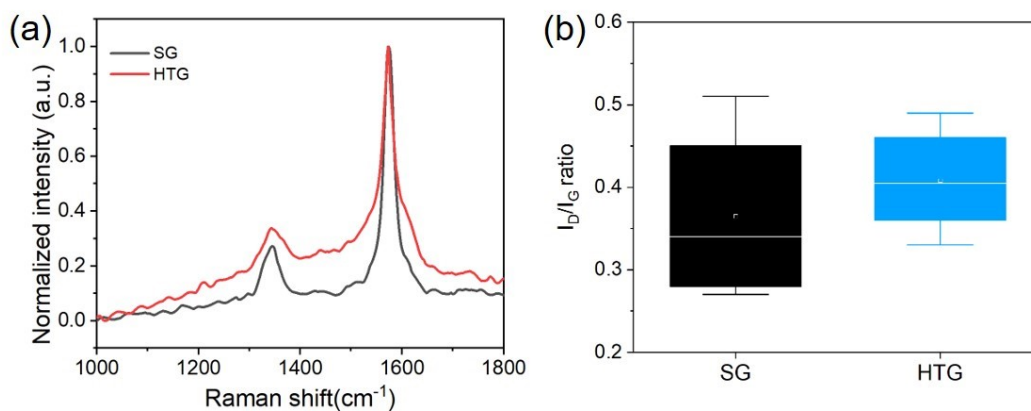


Figure S8. (a) Normalized Raman spectra and (b) I_D/I_G ratio statistical chart of SG and HTG

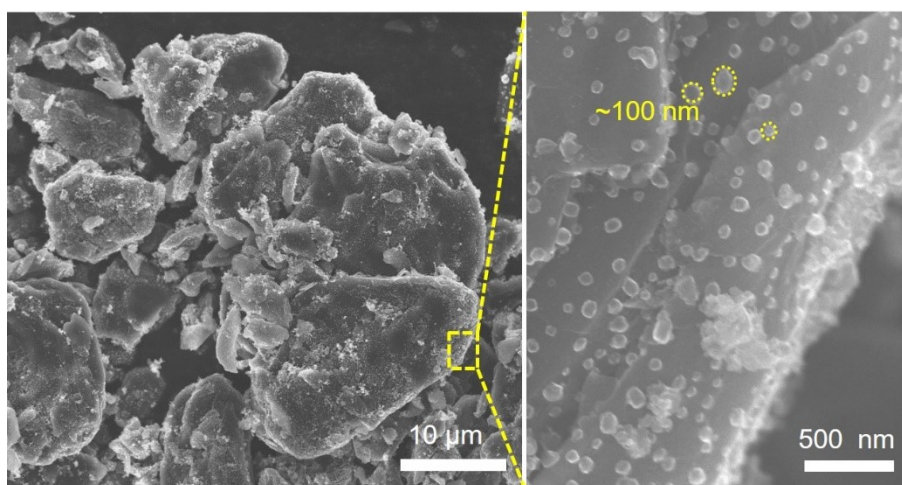


Figure S9. Lots of spherical particles on HTG with a size of ~100 nm.

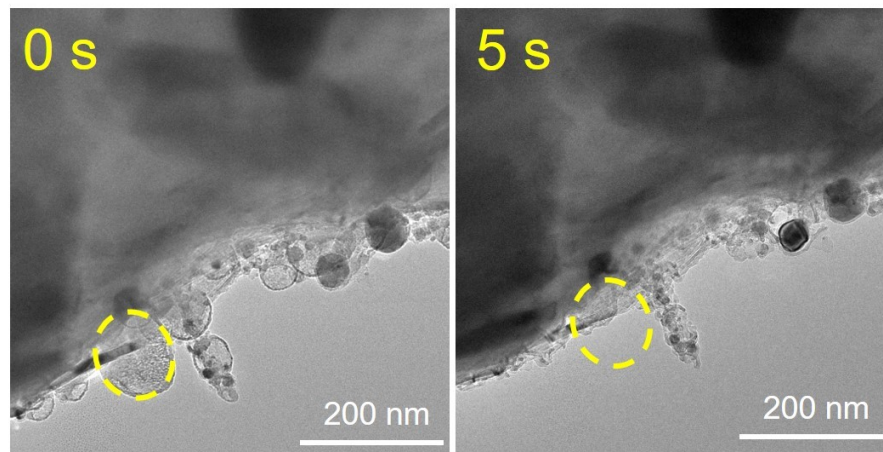


Figure S10. TEM images of HTG before and after electron beam irradiation.

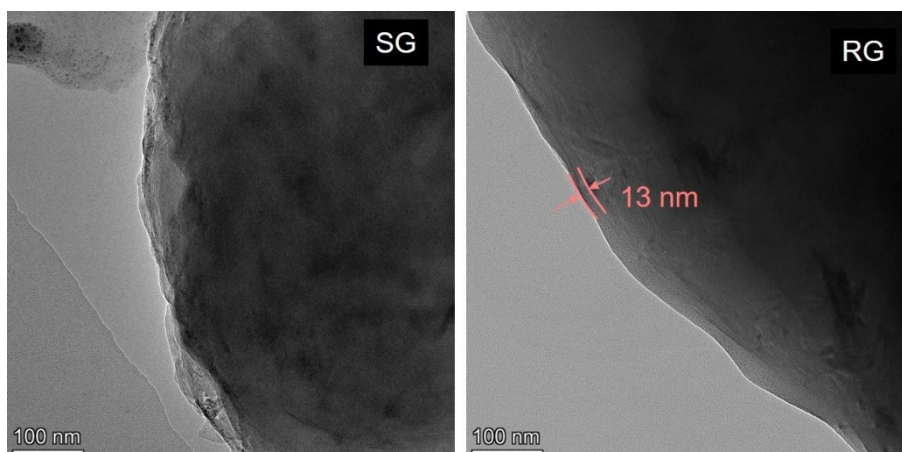


Figure S11. TEM image of SG and RG.

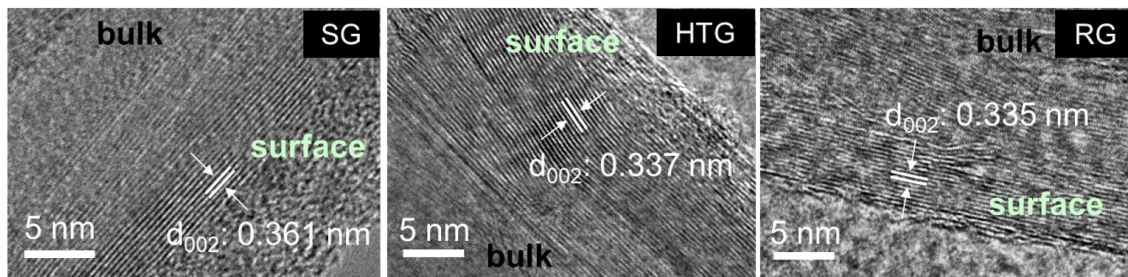


Figure S12. TEM images of SG, HTG, and RG, showing different lattice parameters at the graphite surfaces.

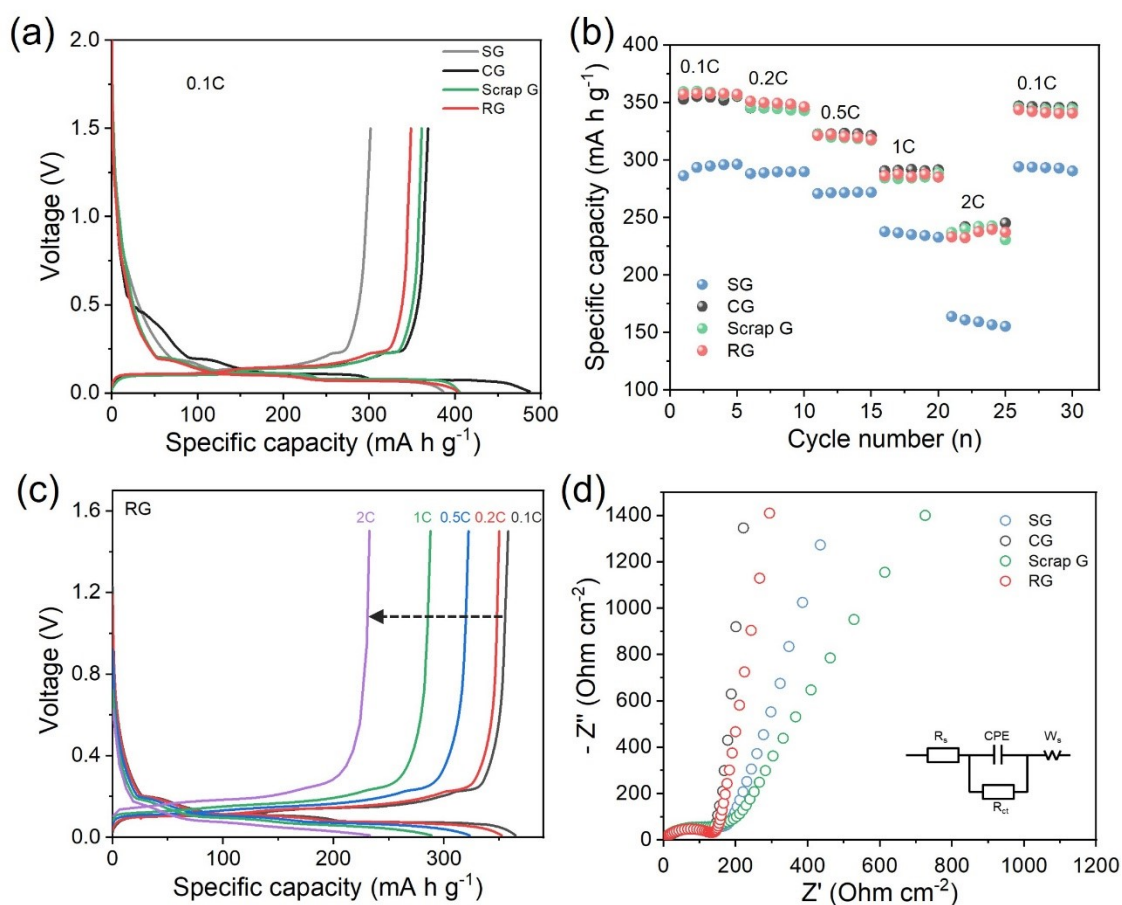


Figure S13. Electrochemical performances of various graphite samples in half-cells. (a) Initial charge and discharge curves at 0.1 C in the range of 0.01–1.5 V and (b) rate capability of SG, CG, RG, and Scrap G. (c) Voltage profiles of RG at different rates from 0.1 to 2 C. (d) Nyquist plots before cycling (insert: the equivalent circuit model) of SG, CG, RG, and Scrap G.

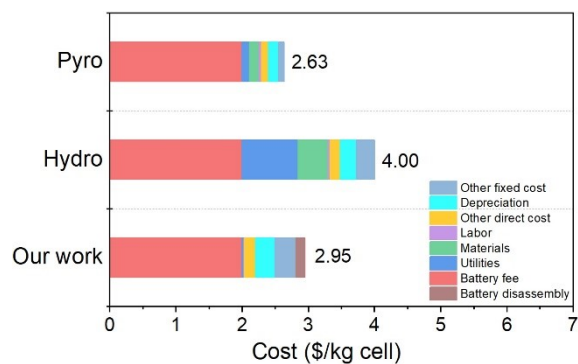


Figure S14. The overall cost of battery recycling.

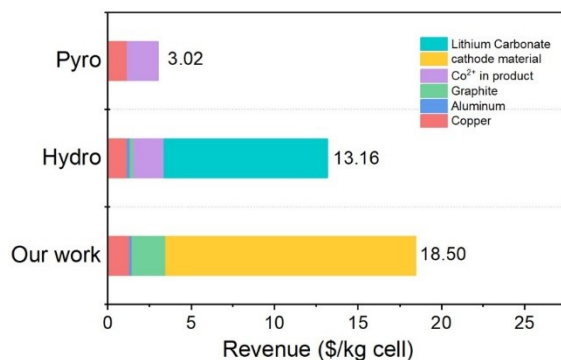


Figure S15. Revenue of battery recycling.

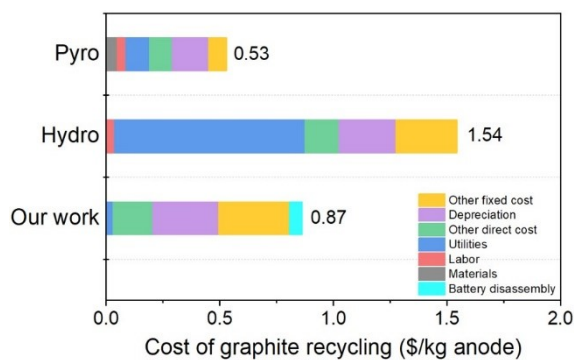


Figure S16. Cost of graphite recycling for different recycling methods.

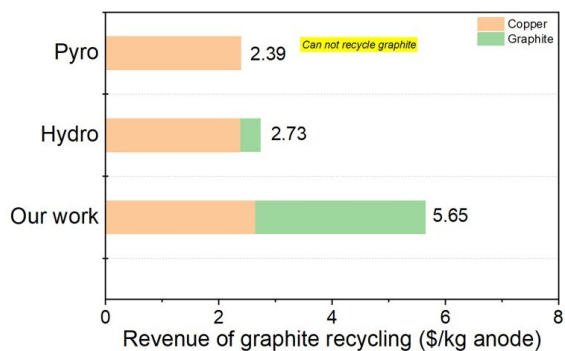


Figure S17. Revenue of graphite recycling for different recycling methods.



Figure S18. Separated copper foil pieces from spent anodes of different battery manufacturers.

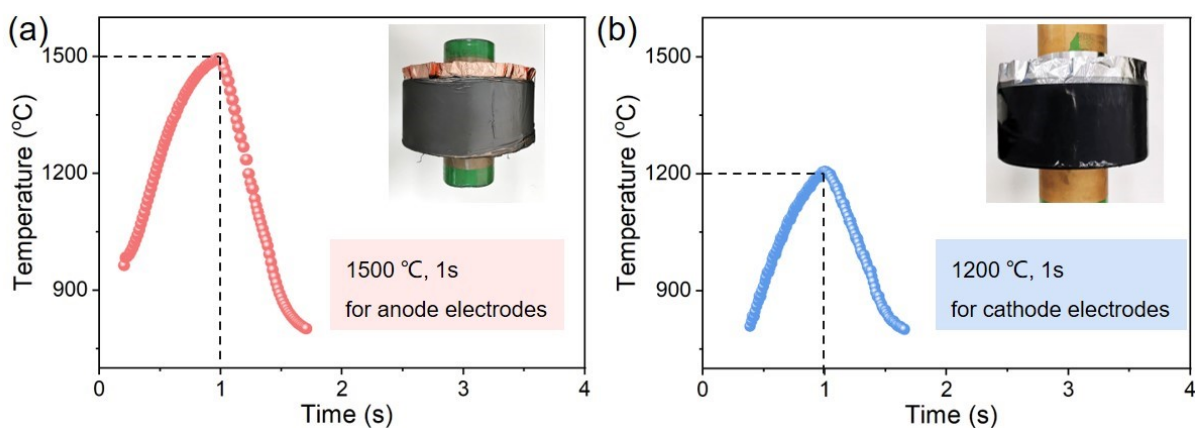


Figure S19. Temperature profiles for the materials recycling from the (a) anode (1500 °C, 1 s) and (b) cathode (1200 °C, 1 s) electrodes, respectively.



Figure S20. Pictures of recycled Al foil and LCO materials via our rolled-over heating method.

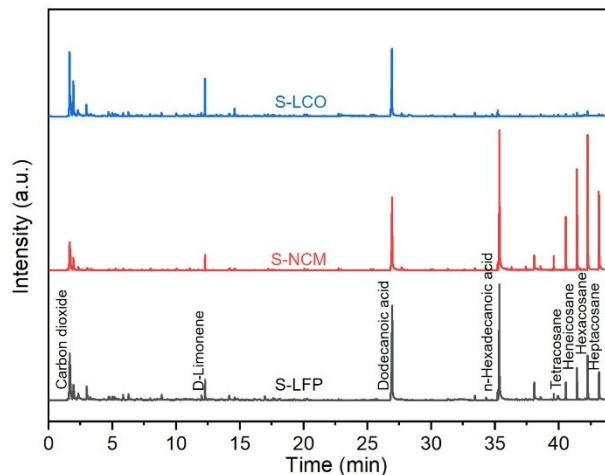


Figure S21. Total ion chromatogram of spent cathodes pyrolyzed in Py-GC/MS, demonstrating the binder decomposed components.

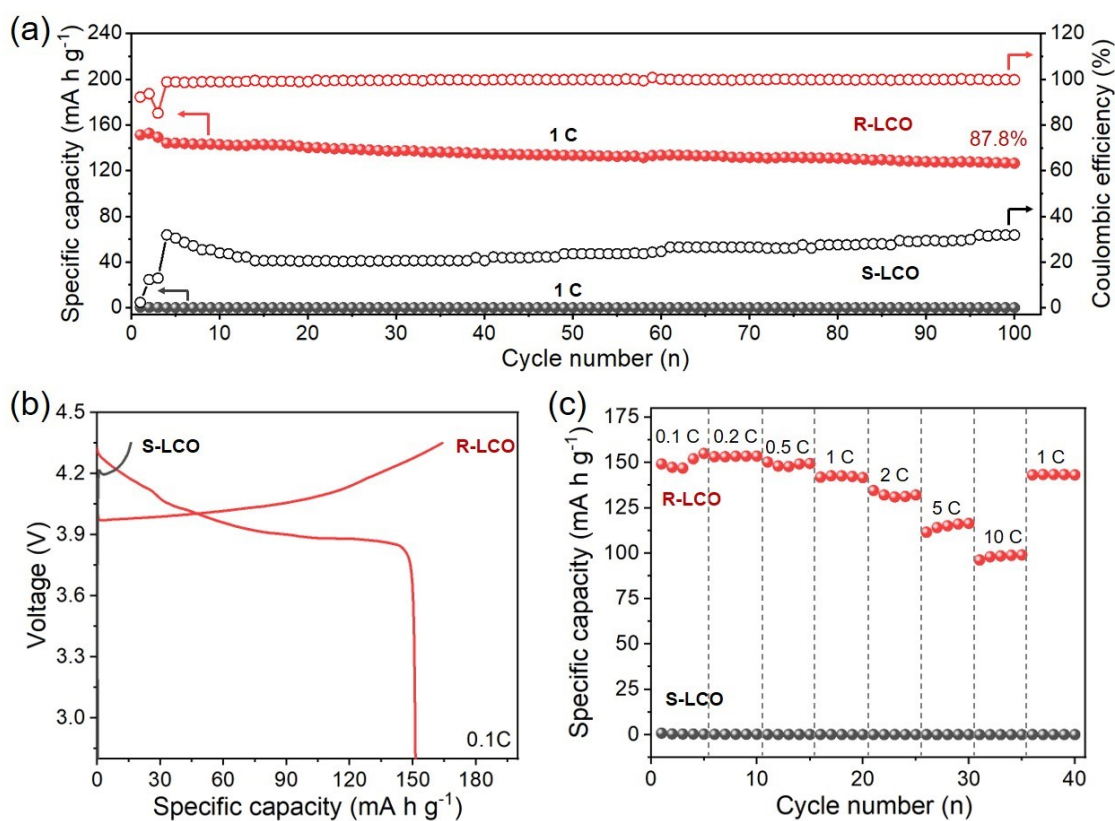


Figure S22. Electrochemical performances of S-LCO and R-LCO samples in half-cells. (a) cycling performance at 1 C after activation at 0.1 C for three cycles, (b) Initial charge and discharge curves at 0.1 C in the range of 2.8–4.35 V, (b) rate capability from 0.1 to 10 C.

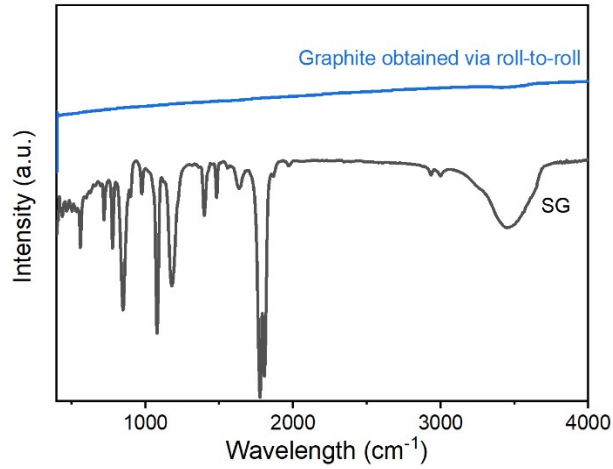


Figure S23. FTIR spectra of SG and the graphite as displayed in Movie S1.

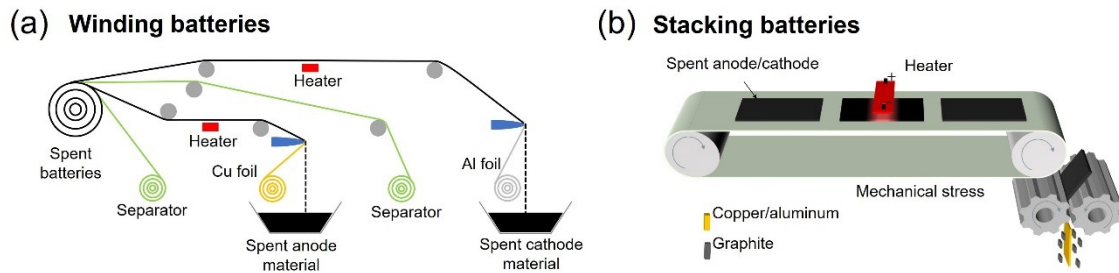


Figure S24. Illustrations of spent electrodes recycling of (a) winding and (b) stacking batteries

Table S1. A summary of all samples prepared in our work.

Category	Abbreviations	Full name	Description of obtaining method
Spent materials	SG	spent graphite	scraped from spent anode manually
	S-LCO	Spent lithium cobalt oxide	scraped from spent LCO cathode electrode manually
	S-NCM	Spent lithium nickel cobalt manganese oxide	scraped from spent NCM cathode electrode manually
	S-LFP	Spent lithium iron phosphate	scraped from spent LFP cathode electrode manually
Recycled materials	HTG	High-temperature graphite	separated from spent anode electrode by shock-type heating
	HT-LCO	High-temperature LCO	separated from spent LCO electrode by shock-type heating
	HT-NCM	High-temperature NCM	separated from spent NCM electrode by shock-type heating
	HT-LFP	High-temperature LFP	separated from spent LFP electrode by shock-type heating
	Scrap G	Scrap graphite	separated from anode scrap by shock-type heating (Note the scrap graphite in Figure 5e is obtained by rolled-over heating)
Regenerated materials	RG	Regenerated graphite	regeneration of HTG through carbon coating following acid cleaning
	R-LCO	Regenerated LCO	regeneration of HT-LCO through sintering following hydrothermal treatment

Table S2. Gas products from pyrolysis of SG.

Peak No.	RT (min)	Area Percentage (%)	Compound
1	1.47	1.62	Phosphoryl fluoride
2	1.61	30.24	Phosphoryl fluoride
3	1.92	0.23	Isoprene
4	4.69	1.50	Toluene
5	7.87	12.60	Styrene
6	10.44	41.50	Ethylene carbonate
7	10.80	0.38	1,4-Dioxaspiro[5.5]undecan-2-one
8	11.00	4.65	Propylene Carbonate
9	12.10	0.72	D-Limonene
10	12.61	0.71	2-Pyrrolidinone, 1-methyl-
11	16.59	1.95	1,2-Oxathiolane, 2,2-dioxide
12	30.98	1.82	Oxalic acid, cyclobutyl pentadecyl ester
13	35.02	2.06	Z-5-Nonadecene

Table S3. The content of impurities in various graphite samples.

Sample	Content of impurities (ppm)			
	Al	Cu	Li	Fe
Mechanical crushing G	5600	72100	5400	
SG	338	5759	3198	152
HTG	117	7122	4130	104
RG	22	3	28	50
Scrap graphite	39	8	2	46

Table S4. Data involved in ICP measurement for various graphite samples

Sample	Sample mass m_0 (g)	Metered volume V_0 (mL)	Impurity element	Concentration of impurity elements in the test solution C_0 (mg/L)	Dilution factor f	Content of impurity elements in sample C_x (ppm)
SG	0.0562	10	Al	1.9017	1	338.37
	0.0562	10	Cu	3.2364	10	5758.75
HTG	0.0540	10	Al	0.6315	1	116.95
	0.0540	10	Cu	3.8459	10	7121.94
RG	0.0474	10	Al	0.1052	1	22.19
	0.0474	10	Cu	0.0163	1	3.45
Scrap G	0.0482	10	Al	0.1890	1	39.20
	0.0482	10	Cu	0.0378	1	7.84

$$C_x(\text{ppm}) = \frac{C_0(\text{mg/L}) * f * V_0(\text{mL})}{m_0(\text{g})}$$

Table S5. Fitting results of EIS spectra of different graphite samples before cycling.

Samples	R_s (Ω)	R_{ct} (Ω)
SG	3.0	168.0
CG	1.4	135.0
Scrap G	1.7	140.8
RG	1.6	135.6

Table S6. Materials requirements (kg) to recycle 1 kg of spent batteries through different recycling technologies

Material inputs (kg)	Pyrometallurgical	Hydrometallurgical	Our transient recycling
Hydrochloric Acid	0.21	0.012	-
Hydrogen Peroxide	0.06	0.366	-
Sodium Hydroxide	-	0.313	-
Limestone	0.3	-	-
Sand	0.15	-	-
Sulfuric Acid	-	1.078	-
Soda Ash	-	0.021	-

Supplementary Movie S1

Automatic separation of anode scrap by roll-to-roll